ACS Photonics

Article

pubs.acs.org/journal/apchd5

Strong Coupling in the Far-Infrared between Graphene Plasmons and the Surface Optical Phonons of Silicon Dioxide

Isaac John Luxmoore,*[,†] Choon How Gan,[†] Peter Qiang Liu,[‡] Federico Valmorra,[‡] Penglei Li,[†] Jérôme Faist,[‡] and Geoffrey R. Nash[†]

[†]College of Engineering, Mathematics and Physical Sciences, University of Exeter, Exeter, EX4 4QF, United Kingdom

[‡]Institute for Quantum Electronics, ETH Zurich, Wolfgang-Pauli-Strasse 16, CH-8093 Zurich, Switzerland

ABSTRACT: We study plasmonic resonances in electrostatically gated graphene nanoribbons on silicon dioxide substrates. Absorption spectra are measured in the mid-far-infrared and reveal multiple peaks, with width-dependent resonant frequencies. We calculate the dielectric function within the random phase approximation and show that the observed spectra can be explained by surface-plasmon−phonon−polariton modes, which arise from coupling of the graphene plasmon to three surface optical phonon modes in silicon dioxide.

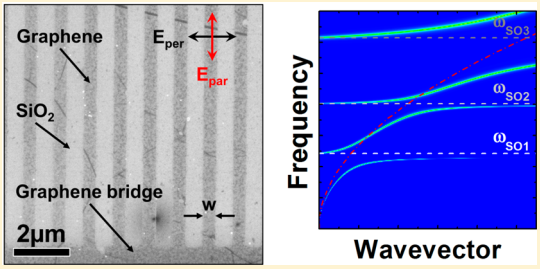

KEYWORDS: *CVD graphene, nanoribbons, plasmonics, infrared spectroscopy*

Graphene has been identified as a potential plasmonic material with resonances in the mid-IR to THz region of the electromagnetic spectrum,[1−7] which provides a wealth of opportunity for technological exploitation in free space communication, security, biosensing, and trace gas detection.[2] The ability to electrostatically gate the charge density in graphene to in excess of 1×10^{13} cm^{-2} predicates tunable and switchable devices[1,4,8,9] and, coupled with an effective mass that is small compared to that of two-dimensional electron gases in conventional semiconductors, results in significantly enhanced light−plasmon coupling and the observation of plasmons at room temperature.[1]

To excite graphene plasmons using light, it is necessary to overcome the momentum mismatch between the surface-plasmon and free-space photons. This can be achieved using near-field excitation, where graphene plasmons have been launched and imaged and shown to have a high degree of electromagnetic confinement.[10,11] Plasmons can also be observed in optical experiments by patterning the graphene into structures with dimensions from 10's of nanometers to several micrometers.[1,4,5,12] Etching graphene into arrays of ribbons allows electromagnetic radiation to excite plasmons with $q \approx (2n + 1)\pi/w$ (where w is the width of the ribbon and $n = 0, 1, 2, ...$), as the incident electric field induces oscillations in the free charge, resulting in the appearance of absorption features in transmission spectra. In micrometer-scale ribbons, the absorption spectrum is determined purely by the plasmon dispersion, with the resonance frequency $\omega_{pl} \propto \sqrt{q}$, lying in the terahertz region.[1] When the ribbon width is reduced to the order of several hundred nanometers, the absorption spectra become more complicated, with multiple resonances in the mid-IR, arising from coupling between the plasmon and optical phonons in the underlying substrate.[5,13]

In this work we investigate the transmission characteristics of electrically contacted nanoribbon arrays, which allow control of the graphene Fermi level via an applied back gate voltage. Four distinct peaks are seen in the transmission spectra, and we show using a calculation of the dielectric function within the random phase approximation (RPA) that this behavior can be attributed to the coupled modes of the graphene plasmon and surface optical phonons of the underlying SiO_2 substrate. We demonstrate coupling of the graphene plasmon to three distinct SO phonon modes, including a resonance at ∼30 μm, which extends graphene plasmonics into the far-infrared part of the electromagnetic spectrum, which is an important region for applications such as chemical and biological spectroscopy.[14,15] With optimization, the devices presented here have the potential to be used as modulators or, with electrical readout, as detectors.[13] In addition, plasmonic waveguides have played an important role in the development of far-infrared quantum cascade laser sources.[16] Finally, we also show that our calculations are consistent with a large range of ribbon widths spanning the frequency range from the THz to mid-infrared.

The devices, pictured in Figure 1a, are fabricated from pretransferred chemical vapor deposited (CVD) monolayer graphene (graphene square) on 300 nm thick SiO_2. The underlying Si substrate is used as a back gate and has a sheet resistance of ∼10 Ωcm. Electron beam lithography and reactive ion etching are used to pattern the graphene into 300 μm × 300 μm nanoribbon arrays with widths between 150 and 500 nm, where the width is ∼40% of the ribbon repeat distance. Cr/Au source and drain contacts are deposited onto the graphene

Received: June 30, 2014
Published: September 17, 2014

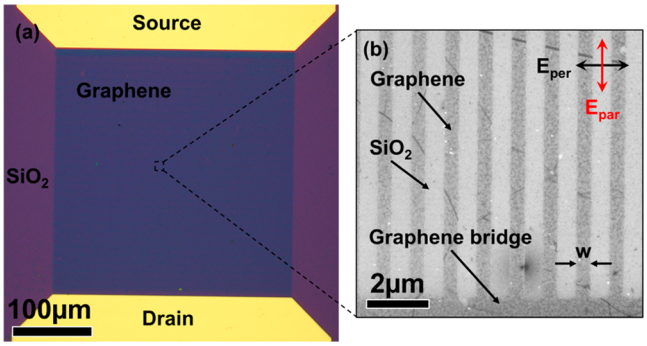

Figure 1. (a) Optical and (b) SEM image of graphene nanoribbon array device. In (b) w indicates the graphene ribbon width and E_{per} (E_{par}) represents the linear polarization of the incident electromagnetic radiation, where the electric field component is perpendicular (parallel) to the nanoribbon.

at either end of the nanoribbon array to allow electrical measurement and biasing. The nanoribbons are connected by 500 nm wide perpendicular bridges every 10 μm to ensure that a small break in an individual nanoribbon does not result in its electrical isolation. Figure 1b shows a scanning electron microscope (SEM) image of a typical graphene nanoribbon device.

Unpatterned graphene devices are also fabricated on the same chip to allow estimation of the mobility and doping of the graphene. Figure 2a shows the field effect characteristic of an

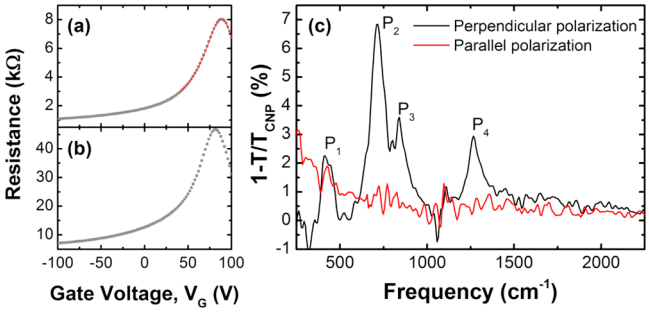

Figure 2. Field effect characteristics of (a) an unpatterned graphene device and (b) a graphene nanoribbon array with a ribbon width of 180 nm. The red line in (a) is a fit to the experimental data following ref 17. (c) Extinction spectra of a 180 nm wide graphene nanoribbon array on SiO_2 for incident light polarized parallel and perpendicular to the ribbons. When the light is polarized perpendicular to the nanoribbon, four peaks, labeled P_1–P_4, are clearly identified.

unpatterned graphene device, where the resistance of the graphene is measured as a function of the voltage applied to the back gate, V_G. This shows behavior typical of monolayer graphene with a peak in resistance at $V_G \approx 88$ V, corresponding to the charge neutral point (V_{CNP}), where the carrier density is minimized. Fitting the experimental data in the voltage range close to V_{CNP} using a phenomenological model[17] allows us to estimate the mobility, μ, to be ~600 $cm^2\ V^{-1}\ s^{-1}$. The large positive value of V_{CNP} indicates that the fabricated samples have a significant intrinsic hole doping, which is also the case for the nanoribbon devices. Figure 2b shows the field effect characteristic for a ribbon array with w = 180 nm, where $V_{CNP} \approx 80$ V. The large intrinsic doping allows wide tuning of the Fermi level, which can be approximated with a simple capacitor model[12] for 300 nm thick SiO_2 as $|E_F| = 0.031(|V_{CNP} - V_G|)^{1/2}$. The resistance is ~5× larger than the unpatterned graphene, suggesting that the mobility is reduced; however, it is difficult to confirm whether this is the case, as the narrow width and relatively long length between bridges means that many ribbons have breaks at some point along their length, thus contributing to an increased resistance.

Infrared spectral transmission measurements were performed in air at room temperature using a home-built infrared microscope coupled to a Fourier transform infrared spectrometer (FTIR) with a measurement range of ~250–6000 cm^{-1}. Collimated light from the FTIR is focused onto the sample using a 36× reflective objective. The transmitted light is collected with a second reflective objective and focused onto a pyro-electric detector using an off-axis parabolic mirror. The incident light is linearly polarized using a broadband wire grid polarizer.

In order to investigate absorption resonances arising from plasmons in the graphene nanoribbons, transmission spectra are measured for a given Fermi level. In the following, we present results for $E_F = -0.37$ eV. The extinction is defined as $1 - T/T_{CNP}$, where T is the transmission spectrum at $E_F = -0.37$ eV and T_{CNP} is the transmission spectrum at the charge neutrality point, $V_G = V_{CNP}$. Such an extinction spectrum is shown in Figure 2c for a nanoribbon with w = 180 nm. When the incident light is polarized parallel to the nanoribbons (E_{par} in Figure 1b), the absorption is not strongly affected by the graphene Fermi level. The only feature in the spectrum is a small increase in the absorption at low frequencies due to the Drude absorption.[1] When the incident light is polarized perpendicular to the nanoribbons (E_{per} in Figure 1b), the absorption is very different, with four sharp absorption resonances revealed, labeled P_1–P_4 in Figure 2c. These absorption resonances can be attributed to the interaction of graphene plasmons with surface optical (SO) phonons[18] in the underlying SiO_2 substrate. Their coupling via the long-range Fröhlich interaction[19] results in the excitation of surface-plasmon–phonon–polariton (SP3) modes.[5,7,12,13,20] In previous work, peaks P_2–P_4 were observed[5,13] due to SO phonon modes at 806 and 1168 cm^{-1}. Here, we report the observation of strong coupling between an additional SO phonon mode at 485 cm^{-1} (ref 20) and the graphene plasmon mode, which results in three distinct anticrossings and four peaks in the measured spectra.

To confirm the origin of P_1, we investigate the absorption spectrum of a range of different nanoribbon widths between 150 and 500 nm. If P_1 does originate from the coupling of the plasmon resonance and a substrate SO phonon, then an anticrossing with P_2 should be observed as the plasmon wavevector, $q = \pi/(w - w_0)$, is tuned by the width of the ribbon, where w_0 is an experimentally determined parameter that accounts for damage at the edge of the ribbons caused by the reactive ion etch.[5,21,22] Figure 3a plots the extinction spectra for several devices with different ribbon widths between 180 and 450 nm. As the ribbon width is increased, all four peaks shift to lower frequency but at different rates, with P_1 and P_2 shifting the most. The spectra are fit with a Fano model,[5,23] and the extracted peak positions are plotted in Figure 3b as a function of q. We take $w_0 = 0$, as the edge damage has been shown to vary considerably,[5,21,22] and we do not determine it experimentally for our devices. The data suggest that there is an anticrossing of P_1 and P_2 at ~485 cm^{-1}, and to confirm that this arises from the plasmon–phonon coupling, we calculate the

dx.doi.org/10.1021/ph500233s | ACS Photonics 2014, 1, 1151–1155

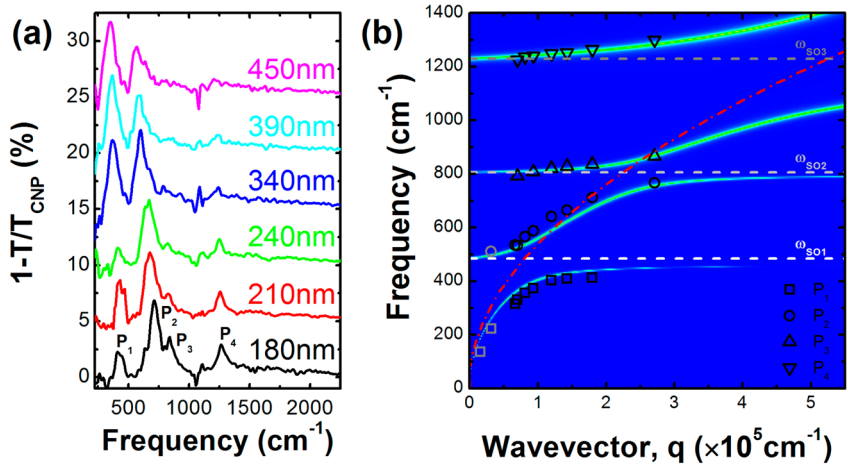

Figure 3. (a) Extinction spectra measured for graphene nanoribbons with a range of widths. (b) Calculated loss plot with extracted peak frequencies overlaid. The red dashed line shows the calculated dispersion of the uncoupled graphene plasmon. The white, light grey and grey dashed lines show the calculated frequency of the three surface optical phonons, ω_{SO1} = 485 cm^{-1}, ω_{SO2} = 806 cm^{-1}, and ω_{SO3} = 1229 cm^{-1}. The gray symbols are peak positions extracted from microribbon arrays and show that the calculations are consistent with a large range of ribbon widths that span a frequency range from the THz to mid-infrared.

dispersion and loss function of the SP3 modes for graphene on a SiO_2 substrate.

The SO phonon frequencies are first obtained by solving the dispersion relation $1 + \epsilon_p(\omega) = 0$, where

$$\epsilon_p(\omega) = \epsilon_\infty + \sum_{n=1}^{N} \frac{f_n \omega_{TO,n}^2}{\omega_{TO,n}^2 - \omega^2} \quad (1)$$

is the ionic dielectric function of an insulator exhibiting N SO phonon modes,[24] ω is the frequency, $\omega_{TO,n}$ is the frequency of the nth transverse optical (TO) phonon mode, and it is assumed that $\omega_{TO,n+1} > \omega_{TO,n}$. In eq 1, $f_n = \epsilon^{(n-1)} - \epsilon^{(n)}$ is the oscillator strength of the nth mode, such that $\sum_{n=1}^{N} f_n = \epsilon_s - \epsilon_\infty$, with $\epsilon_s = \epsilon^{(0)}$ being the static dielectric constant and $\epsilon_\infty = \epsilon^{(N)}$ the high-frequency dielectric constant. It is taken that $\epsilon_s = 3.9$ and $\epsilon_\infty = 2.4$ for the SiO_2 substrate. The values of $\epsilon^{(n)}$ that appear in the oscillator strength f_n were approximated as[24] $\epsilon^{(n)} \approx \epsilon^{(n-1)}(\omega_{TO,n}^2/\omega_{LO,n}^2)$, and the dispersion was calculated from eq 1 for three SO modes (N = 3). In the calculations, the transverse optical (TO) and longitudinal optical (LO) phonon frequencies are taken to be ω_{TO} = [448, 791.7, 1128.1] cm^{-1} and ω_{LO} = [498.6, 811.5, 1317] cm^{-1}, following values obtained from the literature,[25,31] and the SO frequencies ($\omega_{SO,n} \approx \omega_{LO,n}[(\epsilon^{(n)}(\epsilon^{(n-1)} + 1)/\epsilon^{(n-1)}(\epsilon^{(n)} + 1)]^{1/2}$) were found to be [484.8, 805.9, 1229.0] cm^{-1}. The SO mode energies are plotted as dotted lines in Figure 3b and agree well with previous measurements[5,24] and our experimental data. The corresponding ratios of the oscillator coupling strength f_2/f_1 = 1/5 and f_3/f_1 = 4/5 (f_1 = 0.7514) are also in close agreement with our experimental data and previously reported values.[5,24]

To obtain the dispersion of the hybrid SP3 modes, we consider the coupling between a two-dimensional electron gas (the graphene plasmons) and dispersionless SO phonons at zero temperature.[26] Zero-temperature calculations are expected to yield quantitatively accurate results for our measurements taken at room temperature ($T \approx 300$ K, $K_BT \approx 26$ meV), since $E_F \gg K_BT$ and the lowest SO phonon mode energy considered is $\hbar\omega_{SO}^{(min)} \gtrsim 60$ meV. Within the random phase approximation, the total dielectric function is[5,26]

$$\epsilon_{tot}(q, \omega) = 1 - v_F\Pi - \frac{1}{1 + \beta} \quad (2)$$

where $v_F = e^2/(2q\epsilon_\infty\epsilon_0)$ is the 2D Fourier transform of the Coulomb potential, Π is the polarizability of the uncoupled graphene sheet as calculated in ref 27, and

$$\beta = \left[\epsilon_\infty e^{-2qd} \sum_{N}^{n=1} \frac{\alpha_n \omega_{SO,n}^2}{\omega^2 - \omega_{SO,n}^2}\right]^{-1} \quad (3)$$

where the weighted coupling coefficient $\alpha_n = f_n/[(\epsilon^{(n-1)} + 1)(\epsilon^{(n)} + 1)]$ of each mode is proportional to the Fröhlich coupling strength,[19,26] and d is the distance between the graphene and the substrate, taken to be 3.5 Å in the calculations. The loss function is obtained by taking the imaginary part of the inverse dielectric function, i.e., $L = -I(1/\epsilon_{tot})$ (refs 5, 26). The RPA loss function is plotted, along with the uncoupled graphene dispersion and the peak positions from the experimental data, in Figure 3b. We see good agreement between the experimental data and the calculations, confirming that the measured spectra arise from the SP3 modes originating from the coupling of graphene plasmon with three SO phonon modes in the SiO_2 substrate. We additionally plot in Figure 3b the peak positions from microribbon arrays with widths of 1 and 2 μm, fabricated using the same procedure, to show the good agreement between calculations and experiment over a wide frequency range from the THz to mid-infrared.

In the local limit ($\omega \gg \tau^{-1}$ and $\omega \gtrsim v_Fq$, with τ a phenomenological relaxation time for electrons), one may adopt the Drude model to describe the conductivity of monolayer graphene as $\sigma(\omega) = ie^2E_F/(\pi\hbar^2(\omega + i\tau^{-1}))$, which leads to a simplified form of the polarizability:[2,6]

$$\Pi \approx \Pi^{Drude} \approx \frac{2q^2\epsilon_\infty E_F}{\pi^2\hbar^2(\omega^2 + i\omega\tau^{-1})} \quad (4)$$

In general, the dynamical conductivity of graphene has two contributions, intraband (Drude) and interband (see, for example, eqs 4−7 in ref 28). Including the interband contribution is essential when $\hbar\omega > 2E_F$. In our case $\hbar\omega < 2E_F$; therefore the interband conductivity is not taken into

dx.doi.org/10.1021/ph500233s | ACS Photonics 2014, 1, 1151−1155

account. On the basis of calculations of the dispersion of the SP3 modes with Π^{Drude} in eq 2, the Drude approximation was found to be highly accurate for $\omega > 350$ cm^{-1} and nanoribbon widths $w \geq 100$ nm.

The lifetime of the SP3 modes can be extracted from the spectral line width, and we measure values of <100 fs for all four resonances, comparable to previous measurements.[5] For P_1, the lifetime shows a monotonic increase from ∼40 fs to ∼80 fs as the nanoribbon width is reduced from 480 to 180 nm. The increase in lifetime in this range can be explained by the convergence of P_1 and the SO phonon frequency at 485 cm^{-1}, whereby the mode becomes more phonon like.[5] The energy is far below the graphene optical phonon energy (∼0.2 eV), yet the lifetime is still short compared to the SO phonon lifetime of ∼1 ps. The increase in lifetime with decreasing width suggests that edge effects are insignificant and that the lifetime must be dominated by damping mechanisms intrinsic to the graphene. These could be related to impurity[29] and defect scattering,[30] which is consistent with the low mobility, typical of CVD graphene and high doping shown in Figure 2b.

In conclusion, we have experimentally observed plasmonic resonances in graphene nanoribbons. The broad measurement range allows the simultaneous observation of four absorption peaks corresponding to the surface-plasmon−phonon−polariton modes arising from the Fröhlich coupling of graphene plasmons and the three SO phonon modes with frequencies of ∼485, 806, and 1230 cm^{-1}. Coupling to the SO phonon at 485 cm^{-1} pushes graphene plasmonics into the technologically important far-infrared regime, and with improvements in material quality, graphene plasmonics can play an important role in future nanophotonic devices.

AUTHOR INFORMATION

Corresponding Author

*E-mail: i.j.luxmoore@exeter.ac.uk.

Author Contributions

The manuscript was written through contributions of all authors. All authors have given approval to the final version of the manuscript.

Notes

The authors declare no competing financial interest.

ACKNOWLEDGMENTS

The authors would like to thank Sergey Mikhailov for useful discussions and comments on the manuscript. This research was supported by the UK Engineering and Physical Sciences Research Council, via the award of a Fellowship in Frontier Manufacturing (EP/J018651/1) to G.N., and the European Union under the FET-open grant GOSFEL.

REFERENCES

(1) Ju, L.; Geng, B.; Horng, J.; Girit, C.; Martin, M.; Hao, Z.; Bechtel, H. A.; Liang, X.; Zettl, A.; Shen, Y. R.; Wang, F. Graphene plasmonics for tunable terahertz metamaterials. *Nat. Nanotechnol.* **2011**, *6*, 630.

(2) Low, T.; Avouris, P. Graphene plasmonics for terahertz to mid-infrared applications. *ACS Nano* **2014**, *8*, 1086.

(3) Grigorenko, A.; Polini, M.; Novoselov, K. Graphene plasmonics. *Nat. Photonics* **2012**, *6*, 749.

(4) Yan, H.; Li, X.; Chandra, B.; Tulevski, G.; Wu, Y.; Freitag, M.; Zhu, W.; Avouris, P.; Xia, F. Tunable infrared plasmonic devices using graphene/insulator stacks. *Nat. Nanotechnol.* **2012**, *7*, 330.

(5) Yan, H.; Low, T.; Zhu, W.; Wu, Y.; Freitag, M.; Li, X.; Guinea, F.; Avouris, P.; Xia, F. Damping pathways of mid-infrared plasmons in graphene nanostructures. *Nat. Photonics* **2013**, *7*, 394.

(6) Gan, C. H. Analysis of surface plasmon excitation at terahertz frequencies with highly doped graphene sheets via attenuated total reflection. *Appl. Phys. Lett.* **2012**, *101*, 111609.

(7) Fei, Z.; Andreev, G. O.; Bao, W.; Zhang, L. M.; McLeod, A.; Wang, C.; Stewart, M. K.; Zhao, Z.; Dominguez, G.; Thiemens, M.; Fogler, M. M.; Tauber, M. J.; Castro-Neto, A. H.; Lau, C. N.; Keilmann, F.; Basov, D. N. Infrared nanoscopy of Dirac plasmons at the graphene-SiO_2 interface. *Nano Lett.* **2011**, *11*, 4701.

(8) Bludov, Y. V.; Vasilevskiy, M. I.; Peres, N. M. R. Mechanism for graphene-based optoelectronic switches by tuning surface plasmon-polaritons in monolayer graphene. *Europhys. Lett.* **2010**, *92*, 68001.

(9) Chu, H.-S.; Gan, C. H. Active plasmonic switching at mid-infrared wavelengths with graphene ribbon arrays. *Appl. Phys. Lett.* **2013**, *102*, 231107.

(10) Fei, Z.; Rodin, A. S.; Andreev, G. O.; Bao, W.; McLeod, A. S.; Wagner, M.; Zhang, L. M.; Zhao, Z.; Thiemens, M.; Dominguez, G.; Fogler, M. M.; Castro Neto, A. H.; Lau, C. N.; Keilmann, F.; Basov, D. N. Gate-tuning of graphene plasmons revealed by infrared nano-imaging. *Nature* **2012**, *487*, 82.

(11) Chen, J.; Badioli, M.; Alonso-González, P.; Thongrattanasiri, S.; Huth, F.; Osmond, J.; Spasenović, M.; Centeno, A.; Pesquera, A.; Godignon, P.; Zurutuza Elorza, A.; Camara, N.; García de Abajo, F. J.; Hillenbrand, R.; Koppens, F. H. L. Optical nano-imaging of gate-tunable graphene plasmons. *Nature* **2012**, *487*, 77.

(12) Brar, V.; Jang, M. S.; Sherrott, M.; Lopez, J. J.; Atwater, H. A. Highly confined tunable mid-infrared plasmonics in graphene nanoresonators. *Nano Lett.* **2013**, *13*, 2541.

(13) Freitag, M.; Low, T.; Zhu, W.; Yan, H.; Xia, F.; Avouris, P. Photocurrent in graphene harnessed by tunable intrinsic plasmons. *Nat. Commun.* **2013**, *4*, 1951.

(14) Son, J.-H. Terahertz electromagnetic interactions with biological matter and their applications. *J. Appl. Phys.* **2009**, *105*, 102033.

(15) Globus, T. R.; Woolard, D. L.; Samuels, A. C.; Gelmont, B. L.; Hesler, J.; Crowe, T. W.; Bykhovskaia, M. Submillimeter-wave Fourier transform spectroscopy of biological macromolecules. *J. Appl. Phys.* **2002**, *91*, 6105.

(16) Berini, P.; De Leon, I. Surface plasmon−polariton amplifiers and lasers. *Nat. Photonics* **2011**, *6*, 16.

(17) Dorgan, V. E.; Bae, M.-H.; Pop, E. Mobility and saturation velocity in graphene on SiO_2. *Appl. Phys. Lett.* **2010**, *97*, 082112.

(18) Fuchs, R.; Kliewer, K. Optical modes of vibration in an ionic crystal slab. *Phys. Rev.* **1965**, *140*, 2076.

(19) Wang, S. Q.; Mahan, G. D. Electron scattering from surface excitation. *Phys. Rev. B* **1972**, *6*, 4517.

(20) Yan, H.; Xia, F.; Li, Z.; Avouris, P. Plasmonics of coupled graphene micro-structures. *New J. Phys.* **2012**, *14*, 125001.

(21) Berger, C.; Song, Z.; Li, X.; Wu, X.; Brown, N.; Naud, C.; Mayou, D.; Li, T.; Hass, J.; Marchenkov, A. N.; Conrad, E. H.; First, P. N.; De Heer, W. A. Electronic confinement and coherence in patterned epitaxial graphene. *Science* **2006**, *312*, 1191.

(22) Han, M.; Özyilmaz, B.; Zhang, Y.; Kim, P. Energy band-gap engineering of graphene nanoribbons. *Phys. Rev. Lett.* **2007**, *98*, 206805.

(23) Li, Z.; Lui, C.; Cappelluti, H. E.; Benfatto, L.; Mak, K. F.; Carr, G. L.; Shan, J.; Heinz, T. F. Structure-dependent fano resonances in the infrared spectra of phonons in few-layer graphene. *Phys. Rev. Lett.* **2012**, *108*, 156801.

(24) Fischetti, M. V.; Neumayer, D. A.; Cartier, E. A. Effective electron mobility in Si inversion layers in metal−oxide−semiconductor systems with a high-κ insulator: the role of remote phonon scattering. *J. Appl. Phys.* **2001**, *90*, 4587.

(25) Umari, P.; Pasquarello, A.; Dal Corso, A. Raman scattering intensities in α-quartz: a first-principles investigation. *Phys. Rev. B* **2001**, *63*, 094305.

(26) Hwang, E. H.; Sensarma, R.; Das Sarma, S. Plasmon-phonon coupling in graphene. *Phys. Rev. B* **2010**, *82*, 195406.

(27) Hwang, E. H.; Das Sarma, S. Dielectric function, screening, and plasmons in two-dimensional graphene. *Phys. Rev. B* **2007**, *75*, 205418.
(28) Mikhailov, S. A.; Ziegler, K. New electromagnetic mode in graphene. *Phys. Rev. Lett.* **2007**, *99*, 016803.
(29) Langer, T.; Baringhaus, J.; Pfnür, H.; Schumacher, H. W.; Tegenkamp, C. Plasmon damping below the Landau regime: the role of defects in epitaxial graphene. *New J. Phys.* **2010**, *12*, 033017.
(30) Principi, A.; Vignale, G.; Carrega, M.; Polini, M. Impact of disorder on Dirac plasmon losses. *Phys. Rev. B* **2013**, *88*, 121405(R).
(31) Fratini, S.; Guinea, F. Substrate-limited electron dynamics in Graphene. *Phys. Rev. B* **2008**, *77*, 195414.